V.Bratov, S.Kuznetsov, N.Morozov, Seismic barriers filled with solid elastic and granular materials. Comparative analysis, Mathematics and Mechanics of Solids, pp. 1-10. Copyright © 2022 The Author(s). DOI: 10.1177/10812865221104235.

Seismic barriers filled with solid elastic and granular materials. Comparative analysis

V. Bratov [1,3], S. Kuznetsov [4,5,6], N. Morozov [1,2]

[1] Institute of Problems of Mechanical Engineering of Russian Academy of Sciences, Saint-Petersburg, Russia
[2] Saint-Petersburg State University, Saint-Petersburg, Russia
[3] Peter the Great Saint-Petersburg Polytechnic University, Saint-Petersburg, Russia
[4] Moscow State University of Civil Engineering, Moscow, Russia
[5] Bauman Moscow State Technical University, Moscow, Russia
[6] Institute for Problems in Mechanics of Russian Academy of Sciences, Moscow, Russia

e-mail: *vladimir@bratov.com*

Abstract. A comparative study of the vertical seismic barriers intended for protecting from Rayleigh seismic waves and filled with (i) homogeneous linearly elastic materials and (ii) granular metamaterials, is done by the FE modeling. The granular metamaterial obeys the Mohr – Coulomb plasticity model with the associated flow rule, low cohesion value, and small internal friction and dilation angles. The performed numerical analysis reveals a principal ability achieving much higher reduction ratios for magnitudes of accelerations along with much longer shadow zones behind the barrier for barriers filled with metamaterials in comparison with the purely elastic homogeneous barriers.

Keywords: Rayleigh wave; seismic barrier; reduction ratio; Mohr – Coulomb plasticity; cohesion; granular metamaterial

1. Introduction

The current research is aimed at analysing protection properties against Rayleigh seismic waves by two types of the vertical seismic barriers, (i) solid homogeneous elastic barrier, and (ii) barrier filled with a granular metamaterial. The modelling technique utilizes solution of the dynamic outer Lamb problem yielding both Rayleigh surface waves and bulk P and S waves.

1.1. Seismic barriers

The necessity to protect construction sites from action of surface acoustic waves (SAW) among which Rayleigh or Rayleigh – Lamb waves play the most important role, arises quite often [1-3] especially in areas prone to the shallow focus earthquakes [4,5] or for protection from blast loads [6], or traffic loads [7-10]. More rarely, seismic barriers are used for protecting against Love and SH waves [11-13]; the boundary integral equation methods (BIEM) for barriers with elastic anisotropy, are considered in [14].

Nowadays, the several different kinds of seismic barriers protecting against SAW and a more rear evanescent and head waves, are suggested, with vertical barriers being the most common case [7, 15-19]; less frequent horizontal barriers [15, 20]; pile fields intended to scatter the SAW wave energy

[20-22]; and barriers containing periodic or quasi periodic structural members or metamaterials acting as a phononic crystal [23-26]. The principal ideas for the use of seismic barriers relate to reflection, refraction, scattering and dissipation energy; the latter mainly refers to the metamaterials with significant inelastic response, and especially to the granular metamaterials.

Quite a large number of works concerns the pile fields for scattering Rayleigh waves and thus, protecting the region surrounded by the pile field [27-29]. Presumably, this type of barriers can be considered as the most cost efficient comparing with the other types of seismic barriers [30, 31].

1.2. Mathematical models for granular metamaterials

There are several mathematical models that are used for granular materials; among others hyperelastic, elastic and hypoelastic models should be mentioned, as well as elastic-plastic models, models utilizing the discrete element methods, and hydrodynamic models. Some of the most common methods and models are considered in more detail below. As the literature review given below shows, the continuous plasticity models can be considered as the most appropriate candidates for modeling granular metamaterials, however, some other continuous models are developed; these are hyperelastic, hypoelastic, hydrodynamic and various elastic-plastic models.

1.2.1. Hyperelastic models. Even at strong ground motions caused by the severe earthquakes, the strain tensor is assumed infinitesimal in the areas containing no faults [32]:

$$\boldsymbol{\varepsilon} \equiv \mathrm{sym}\left(\mathbf{F}\right) \approx \frac{1}{2}\left(\nabla \mathbf{u} + \nabla \mathbf{u}^T\right), \tag{1.1}$$

where $\mathbf{F}$ is the strain, and $\mathbf{u}$ is the displacement field, the stress-strain relation for a hyperelastic material can be written in a form [33]:

$$\boldsymbol{\sigma} = \lambda(I_{\boldsymbol{\varepsilon}}, II_{\boldsymbol{\varepsilon}}, III_{\boldsymbol{\varepsilon}}) I_{\boldsymbol{\varepsilon}}\, \mathbf{I} + 2\mu(I_{\boldsymbol{\varepsilon}}, II_{\boldsymbol{\varepsilon}}, III_{\boldsymbol{\varepsilon}})\boldsymbol{\varepsilon}, \tag{1.2}$$

Herein, $\mathbf{I}$ is the unit matrix (tensor); the material functions λ and μ depend solely upon strain invariants

$$I_{\boldsymbol{\varepsilon}} \equiv \mathrm{tr}(\boldsymbol{\varepsilon}), \quad II_{\boldsymbol{\varepsilon}} \equiv \tfrac{1}{2}\left(I_{\boldsymbol{\varepsilon}}^2 - \boldsymbol{\varepsilon}\cdot\cdot\boldsymbol{\varepsilon}\right), \quad III_{\boldsymbol{\varepsilon}} \equiv \det(\boldsymbol{\varepsilon}), \tag{1.3}$$

herein, the double dot means the convolution with respect to two indices. In addition to Eq. (1.2) for a hyperelastic material it is assumed there is an elastic potential $\Psi(I_{\boldsymbol{\varepsilon}}, II_{\boldsymbol{\varepsilon}}, III_{\boldsymbol{\varepsilon}})$ satisfying a relation [34, 35]:

$$\boldsymbol{\sigma} = \nabla_{\boldsymbol{\varepsilon}} \Psi(I_{\boldsymbol{\varepsilon}}, II_{\boldsymbol{\varepsilon}}, III_{\boldsymbol{\varepsilon}}), \tag{1.4}$$

where ∇_{ε} denotes the derivative with respect to ε. With account of (1.3), Eq. (1.4) takes the form (Ericksen, 1960)

$$\boldsymbol{\sigma} = \frac{\partial \Psi}{\partial I_{\boldsymbol{\varepsilon}}}\mathbf{I} + \frac{\partial \Psi}{\partial II_{\boldsymbol{\varepsilon}}}\left(I_{\boldsymbol{\varepsilon}}\mathbf{I} - \boldsymbol{\varepsilon}\right) + \frac{\partial \Psi}{\partial III_{\boldsymbol{\varepsilon}}}\left(\boldsymbol{\varepsilon}\cdot\boldsymbol{\varepsilon} - I_{\boldsymbol{\varepsilon}}\boldsymbol{\varepsilon} + II_{\boldsymbol{\varepsilon}}\mathbf{I}\right). \tag{1.5}$$

Now, combining Eqs. (1.2), (1.5) yields

$$\begin{aligned} \lambda(I_{\boldsymbol{\varepsilon}}, II_{\boldsymbol{\varepsilon}}, III_{\boldsymbol{\varepsilon}}) &= \frac{\partial \Psi}{\partial I_{\boldsymbol{\varepsilon}}} I_{\boldsymbol{\varepsilon}}^{-1} + \frac{\partial \Psi}{\partial II_{\boldsymbol{\varepsilon}}} + \frac{\partial \Psi}{\partial III_{\boldsymbol{\varepsilon}}} II_{\boldsymbol{\varepsilon}} I_{\boldsymbol{\varepsilon}}^{-1} \\ 2\mu(I_{\boldsymbol{\varepsilon}}, II_{\boldsymbol{\varepsilon}}, III_{\boldsymbol{\varepsilon}}) &= -\frac{\partial \Psi}{\partial II_{\boldsymbol{\varepsilon}}} + \frac{\partial \Psi}{\partial III_{\boldsymbol{\varepsilon}}}\left(\boldsymbol{\varepsilon}^{-1} - I_{\boldsymbol{\varepsilon}}\right) \end{aligned}. \tag{1.6}$$

While hyperelastic models are quite often used for modeling wave propagation in granular media [34, 36], their major shortcoming associates with the absence of energy dissipation at cyclic motions, containing the compression – decompression phases.

1.2.2. Hypoelastic models. According to Truesdell [37] the stress tensor infinitesimal increment $d_{\tau}\boldsymbol{\sigma}(\mathbf{x}, \tau)$ can be defined by the strain tensor infinitesimal increment $d_{\tau}\boldsymbol{\varepsilon}(\mathbf{x}, \tau)$, where τ is

the time-like parameter. Assuming, as before, that the strain tensor is infinitesimal, the constitutive relation for an isotropic hypo-elastic material takes the form

$$d_\tau \boldsymbol{\sigma} = \lambda(I_{\boldsymbol{\sigma}}, II_{\boldsymbol{\sigma}}, III_{\boldsymbol{\sigma}}) I_{d\boldsymbol{\varepsilon}}\, \mathbf{I} + 2\mu(I_{\boldsymbol{\sigma}}, II_{\boldsymbol{\sigma}}, III_{\boldsymbol{\sigma}}) \cdot d_\tau \boldsymbol{\varepsilon}\,, \tag{1.7}$$

where $I_\sigma, II_\sigma, III_\sigma$ are the corresponding stress invariants, defined similarly to (1.3).
It is also known [38] that the special triggering mechanism can be incorporated into Eq. (1.7) to achieve different mechanisms at loading and unloading; that turns the considered hypoelastic models into elastic-plastic models.

The equation of motion for hypoelastic models are often written in the incremental form

$$\nabla_{\mathbf{x}} \cdot \left(d_\tau \boldsymbol{\sigma} \right) + d_\tau \left(\rho \mathbf{b} \right) = d_\tau \left(\rho \mathbf{v} \right), \tag{1.8}$$

where $\mathbf{v}$ is the velocity field, ρ is the material density, and $\mathbf{b}$ is the body force field. The hypoelastic model defined by the equation of state (1.7) is quite often used for modeling wave propagation in granular media; see [39, 40].

1.2.3. Hydrodynamic models and discrete element methods. The granular media are sometimes modeled by hydrodynamic equations of state; see [41-46]. The space-average hydrodynamic equations of motion for the granular medium can be derived by the Chapman – Enskog method [47] and written in the form [51]:

$$\begin{aligned} &\partial_\tau n + \mathrm{div}_{\mathbf{x}} \left(n\mathbf{v} \right) = 0 \\ &n\left(\partial_\tau \mathbf{v} + \mathbf{v} \cdot \nabla_{\mathbf{x}} \mathbf{v} \right) = -\mathrm{div}_{\mathbf{x}} \mathbf{P} + n\mathbf{F} \\ &n\left(\partial_\tau T + \mathbf{v} \cdot \nabla_{\mathbf{x}} T \right) = -\mathrm{div}_{\mathbf{x}} \mathbf{q} - \mathbf{P} \cdot\cdot \nabla_{\mathbf{x}} \mathbf{v} - nT\varsigma \end{aligned}, \tag{1.9}$$

where n is the number density field; $\mathbf{v}$ is the velocity field; T is the temperature field; $\mathbf{F}$ is the external number density (body) force; $\mathbf{P}$ is the pressure (tensor) field; $\mathbf{q}$ is the heat flux; ς is the specific loss of mechanical energy. To accomplish balance equations (1.9) the following relations for the pressure tensor, heat flux and the specific mechanical energy dissipation are suggested [42, 43]:

$$\begin{aligned} &\mathbf{P} = p\mathbf{I} - \eta\left(\nabla_{\mathbf{x}} \mathbf{u} + \nabla_{\mathbf{x}} \mathbf{v} - \left(\mathrm{div}_{\mathbf{x}} \mathbf{v} \right) \mathbf{I} \right) - \gamma \left(\mathrm{div}_{\mathbf{x}} \mathbf{v} \right) \mathbf{I} \\ &\mathbf{q} = -\kappa \nabla_{\mathbf{x}} T - \mu \nabla_{\mathbf{x}} n \\ &\varsigma = \varsigma_0 + \varsigma_1 \mathrm{div}_{\mathbf{x}} \mathbf{v} \end{aligned}, \tag{1.10}$$

where p is the hydrostatic pressure; η is the shear viscosity, γ is the bulk viscosity; κ is the thermal conductivity coefficient; μ is the additional parameter specifying dependence of the heat flux on the number density gradient; the last expression for the specific mechanical energy loss is known as the Goldstein – Shapiro equation [44].

Equations (1.9), (1.10) form the closed form system of hyperbolic equations, solved either by the finite difference algorithms; see [48,49]; or the discrete element methods (DEM); see [45-48]. Sometimes, hydrodynamic models are used within the meshfree smooth particle hydrodynamics (SPH) method; in this regard see [54-56].

1.2.4. General elastic-plastic models. The elastic-plastic models are quite often used for analyzing wave propagation in granular media [57-60]. Within these models, the usual approach is to split the infinitesimal strain into recoverable elastic ($\boldsymbol{\varepsilon}_e$) and unrecoverable plastic ($\boldsymbol{\varepsilon}_{pl}$) part:

$$\boldsymbol{\varepsilon} = \boldsymbol{\varepsilon}_e + \boldsymbol{\varepsilon}_{pl}\,. \tag{1.11}$$

Assuming, the considered materials are isotropic, both strain and stress tensors are split into spherical and deviatoric parts

$$\begin{aligned} &\boldsymbol{\sigma} = -p\mathbf{I} + \mathbf{d}_\sigma, \quad p = -\tfrac{I_\sigma}{3}, \quad \mathbf{d}_\sigma = \boldsymbol{\sigma} + p\mathbf{I} \\ &\boldsymbol{\varepsilon} = \tfrac{\theta}{3}\mathbf{I} + \mathbf{d}_\varepsilon, \quad \theta = I_\varepsilon, \quad \mathbf{d}_\varepsilon = \boldsymbol{\varepsilon} - \tfrac{\theta}{3}\mathbf{I} \end{aligned}, \tag{1.12}$$

herein, p is pressure; θ is the volumetric strain, and $\mathbf{d}$ stands for the corresponding deviatoric tensor.

For the theories with a single yield surface, the yield surface is defined by an equation written in terms of the corresponding invariants:

$$f(I_\sigma, II_\sigma, III_\sigma) = 0. \tag{1.13}$$

where f is a convex function. If f is independent of the third invariant, then Eq. (1.13) can be rewritten, as

$$f(p, q_\sigma) = 0, \tag{1.14}$$

where q_σ is one of the equivalent measures in the deviatoric space. Quite often in mechanics of granular materials [61-65] the function f is considered as a potential for the velocity (increment) of the plastic strain

$$\dot{\boldsymbol{\varepsilon}}_{pl} = \dot{\lambda}\nabla_{\boldsymbol{\sigma}} f. \tag{1.15}$$

Parameter $\dot{\lambda}$ determines velocity of the plastic strain.

1.2.5. Mohr – Coulomb plasticity model. The Mohr – Coulomb plasticity model is apparently the most popular in mechanics of granular materials, see [15, 33, 66-68]. This model will be used in analyzing energy dissipation and scattering by seismic barriers filled with the granular metamaterials. It should also be noted that while most of solid elastic-plastic materials may exhibit degradation of their mechanical properties at cyclic loadings, especially those exceeding the limiting yield stress [65], the considered granular metamaterials are free from this kind of degradation, since the individual granules have actually no chemical bonding forces [67].

Within Mohr – Coulomb plasticity models, the deviatoric semi-norm q_σ is taken as

$$q_\sigma = \sigma_1 - \sigma_3, \tag{1.16}$$

where σ_1 and σ_3 are correspondingly the maximal and minimal principal stresses. The Mohr – Coulomb plasticity model is based on the linear relation between pressure p and the deviatoric semi-norm q_σ

$$q_\sigma = c + p\tan\varphi, \tag{1.17}$$

where c is the parameter, known as cohesion, it corresponds to the yield stress at the zero pressure value; angle φ is known as the angle of the internal dry friction; and the internal dry friction is independent of the speed of strain. Thus, the yield surface (1.14) for the Mohr – Coulomb plasticity model becomes a pyramid; and as Eq. (1.17) shows, the f -function in (1.14) depends upon the unique variable parameter q_σ or p. The pyramid apex along the p -axis is located at

$$p = -\frac{c}{\tan\varphi}, \tag{1.18}$$

Note also, that according to Eq. (1.17) at vanishing φ the pyramid is becoming a prism without the apex point.

In case of the non-associative flow rule, the dilation angle $\psi \neq \varphi$; herein, the dilation angle characterizes deflection of vector $\nabla_{\boldsymbol{\sigma}} f$ from the deviatoric plane $\mathbf{d}_\sigma$. By denoting the unit normal to the deviatoric plane by $\boldsymbol{\nu}_{\mathbf{d}_\sigma}$ the following expression for the dilation angle can be derived, as

$$\psi = \frac{\pi}{2} - \arctan\left(\frac{\mathbf{v}_{\mathbf{d}_\sigma} \cdot \mathbf{Q} \cdot \nabla_{\boldsymbol{\sigma}} f}{\|\nabla_{\boldsymbol{\sigma}} f\|} \right) \tag{19}$$

Herein, $\mathbf{Q}$ is the rotation (second order) tensor characterizing deflection of the dilation angle from the internal friction angle φ; note also, that

$$\varphi = \arctan\left(\frac{\nabla_{\boldsymbol{\sigma}} f}{\|\nabla_{\boldsymbol{\sigma}} f\|} \right). \tag{1.20}$$

In the following sections the associative flow rule ($\varphi = \psi$) will be adopted.

2. Numerical calculations

Protective capacity of seismic barriers made of material exhibiting linear elastic behavior and granular metamaterial simulated as Mohr-Coulomb material is analyzed. Utilizing LS-DYNA [69] finite element commercial software, a problem for a dynamically loaded halfplane with embedded protective barrier is solved utilizing explicit time integration. Problem geometry is given in figure 1.

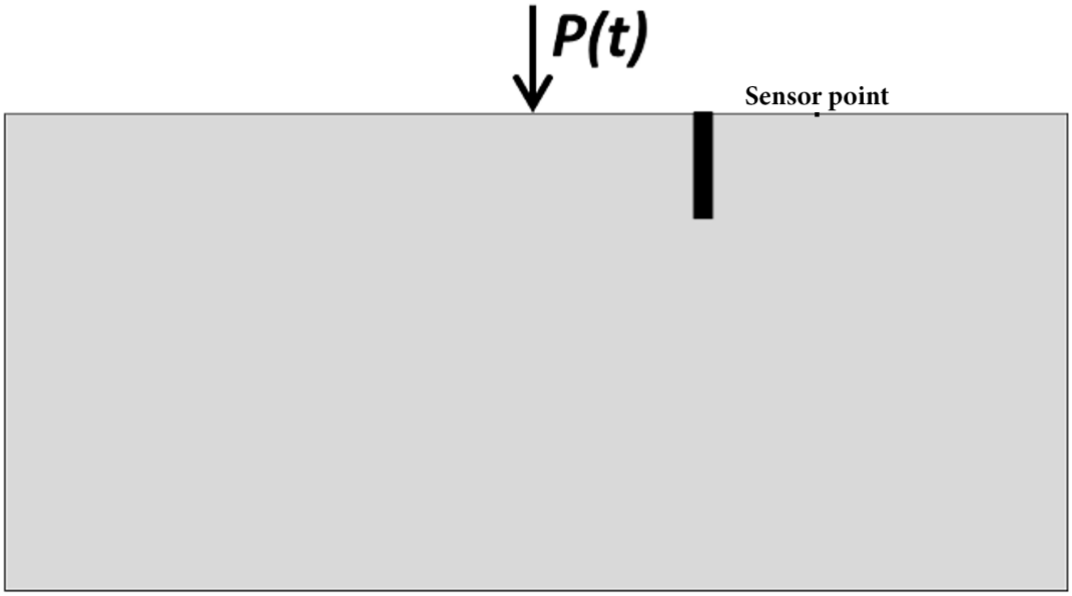

Figure 1. Numerical solution geometry

The load *P(t)* is applied as a concentrated force at the surface at *x=0*. The time dependence of force used in the following simulations is given graphically in figure 2. Force amplitude P_{peak}=1000*N*.

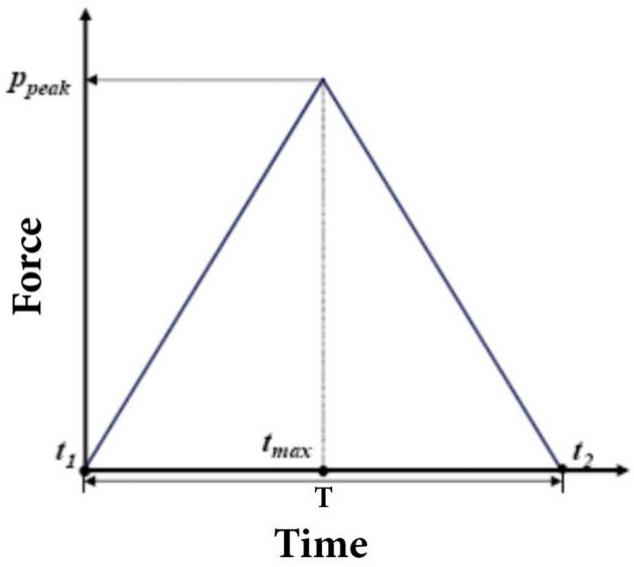

Figure 2. Time shape of P(t) used in simulations.

The load duration *T* is chosen to be equal to the time needed for the fastest (longitudinal) wave to travel distance equal to the barrier depth in the material representing half-space. There's no doubt that the load duration will significantly affect wave interaction with a barrier of a prescribed geometry and, hence, will have a substantial effect on the effective barrier protective properties. It is apparent, that barriers with sizes significantly smaller than the oncoming wave wavelength, cannot have notable influence on the passing wave. Waves with wavelengths comparable or smaller than the barrier size can be significantly transformed in the process of interaction with the barrier. Credibly, the waves with wavelengths substantially smaller than the barrier dimensions can be affectively filtered by the barrier with no pronounce dependency on the wavelength. Thereby, the most interesting (from both, the theoretical and the practical point of view) is the case of waves with wavelength comparable to dimensions of the protective barrier.

For each of the tested barrier materials maximum overtime displacement induced by the load *P(t)* in the sensor point (see figure 1) is scaled with the magnitude of displacement in the same point for the case with no seismic barrier to receive protection factor for the corresponding barrier type. For example, protection factor equal to 2.0 means that the magnitude of displacements in the sensor point is reduced by the factor of 2.

The media is simulated as a linear elastic material with the properties typical for soil – elastic modulus, E=30 *MPa*, density, ρ=1750 kg/m^3, Poisson's ratio, ν=0.3. As demonstrated before (see. ex. [15]) vertical seismic barriers made of linear elastic materials can be successfully utilized to reduce vibrations induced by remote loads. Within the framework of the developed model two cases of linear elastic barrier were calculated: barrier made of a material that is much stiffer than the media (material with properties typical for concrete - E=30 *GPa*, ρ=2400 kg/m^3, Poisson's ratio, ν=0.35) and much softer that the media (material with properties typical for expanded polystyrene (EPS) geofoam - E=3 *MPa*, ρ=15 kg/m^3, Poisson's ratio, ν=0.12). The corresponding protection factors were found to be **2.2** for the case of seismic barrier made of concrete and **1.86** for the case of seismic barrier made of EPS geofoam.

In order to investigate potential protective properties of granular metamaterials, Mohr-Coulomb material model was used as a model for barrier media. The following properties for Mohr-Coulomb model were adopted: shear modulus, *G*=20 *MPa*, density, ρ=2000 kg/m^3, Poisson's ratio, ν=0.25. As the associative flow is adopted, angles $\varphi = \psi$ are equal. Figure 3 plots the received

protection factor as a function of angle φ. Cohesion c in this case is equal to 625 kPa, but this value does not have any significant meaning as that should be scaled with the amplitude of the load $P(t)$.

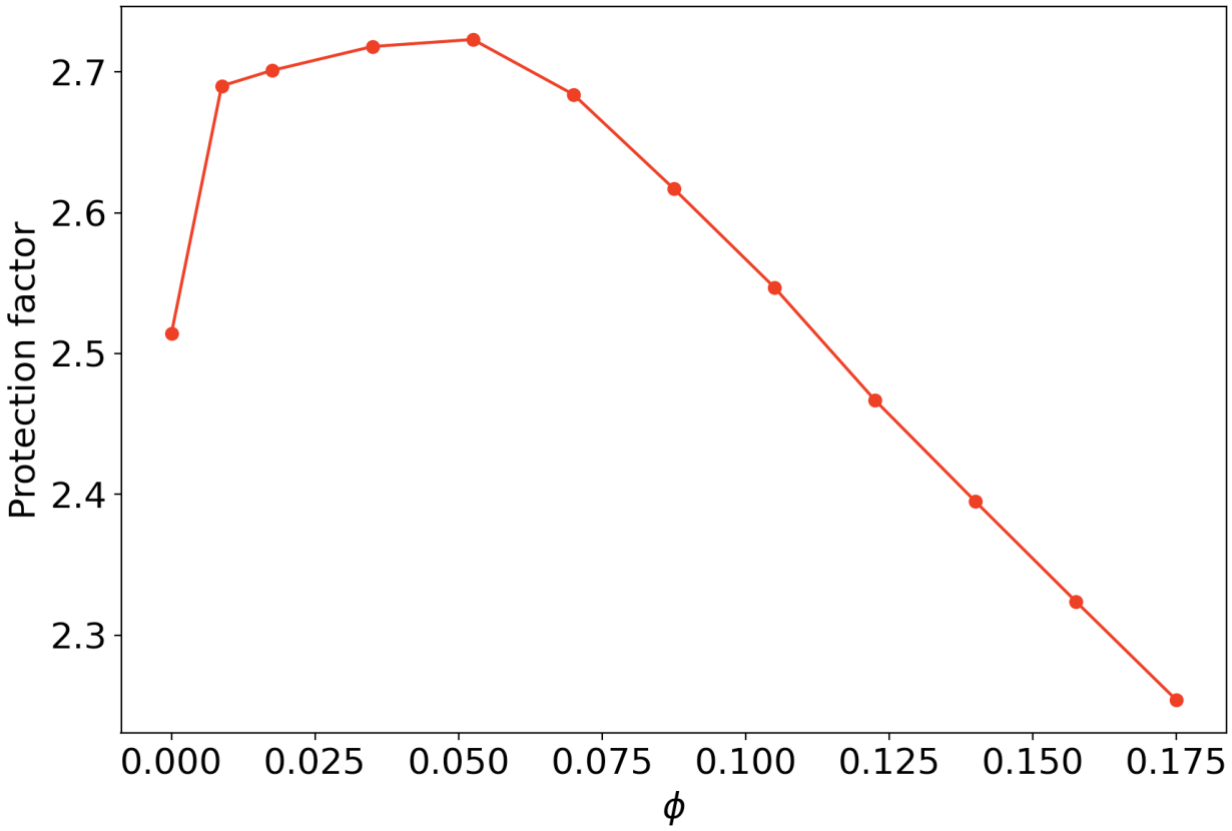

Figure 3. Barrier protection factor as a function of angle φ. Angle is measured in radians. Cohesion, c=625 *kPa*.

As follows from figure 3, there exist an optimal value for friction angles. For small (less than 5 degrees) angles protection factors can attain values of 2.7-2.8 significantly outperforming the protection of linear elastic barriers. For larger values of friction angle φ the barrier behavior is getting closer to elastic material as it gets more difficult for plasticity to onset. For very small values of angle φ, the plasticity is getting very easy to onset and dissipation of energy into this plastic deformation is decreasing. The interplay of these two processes is determining the exitance of optimal value for friction angles.

The effect of cohesion value on the barrier protection factor was also studied. Figure 4 is giving attained protection factors as a function of cohesion value for three different values of friction angle φ. Cohesion is measured in *kPa*, but once again it should be noted that the cohesion value does not have a significant meaning as that should be scaled with the amplitude of the load *P(t)*.

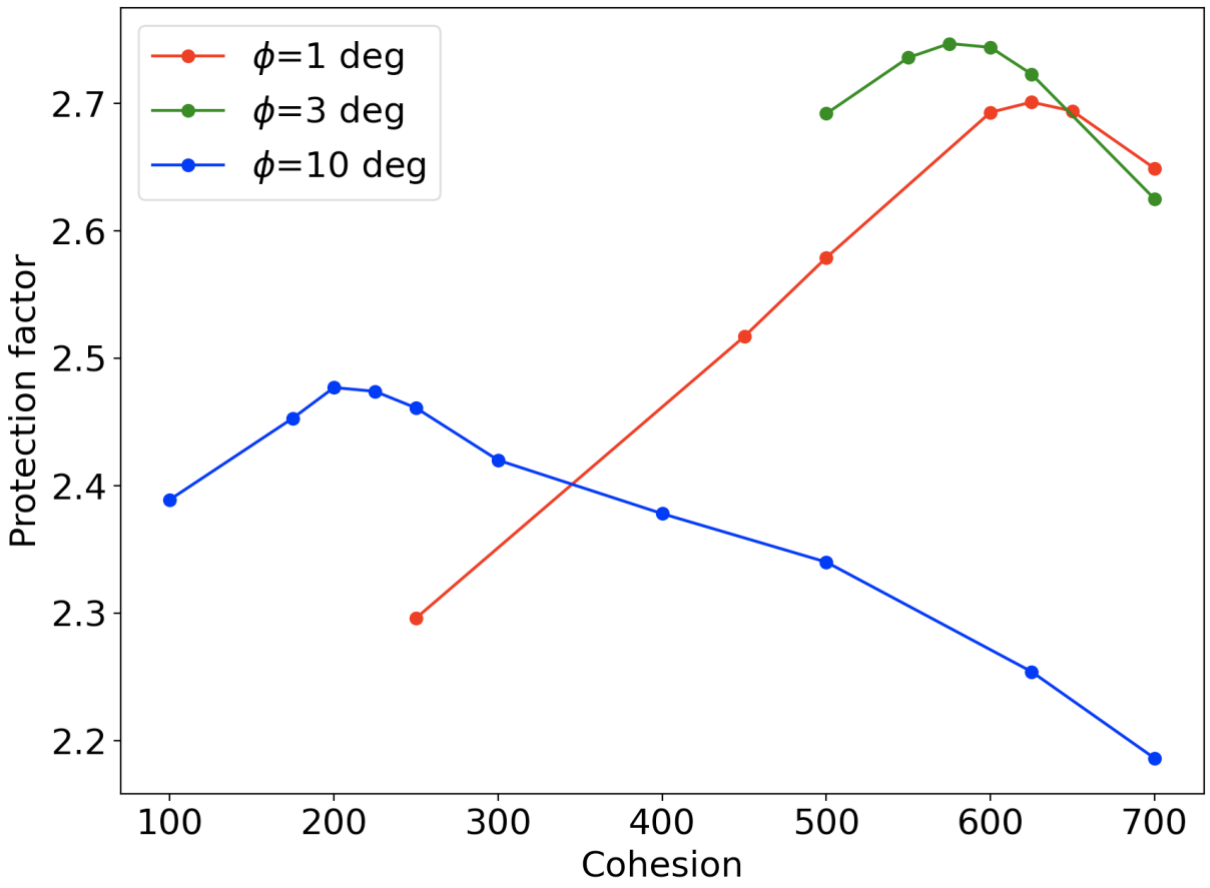

Figure 4. Barrier protection factor as a function of cohesion value. Cohesion is measured in *KPa*.

As evident from figure 4, for every of the three studied friction angle values there exists an optimal value of cohesion (that is obviously also a function of the load amplitude). Large cohesion values are making plastic deformation of the barrier material more difficult to onset, making material behavior more linear-elastic. Very small cohesion values are resulting in exiguous resistance to shear, resulting in loss of energy dissipation into plastic deformation. The interplay between these two processes is determining the exitance of optimal cohesion value. As demonstrated by the simulation, material following the Mohr – Coulomb model can significantly outperform linear elastic materials in terms of vibration protection properties. It should be noted, that linear-elastic barrier behaviour can be received as a limit for large cohesion values in Mohr-Coulomb material model. It was checked (see ex. figure 5) that for larger cohesion stresses the received protection factor is monotonously decreasing, reaching the value that is received for exact linear-elastic equivalent (i.e., with the same elastic properties).

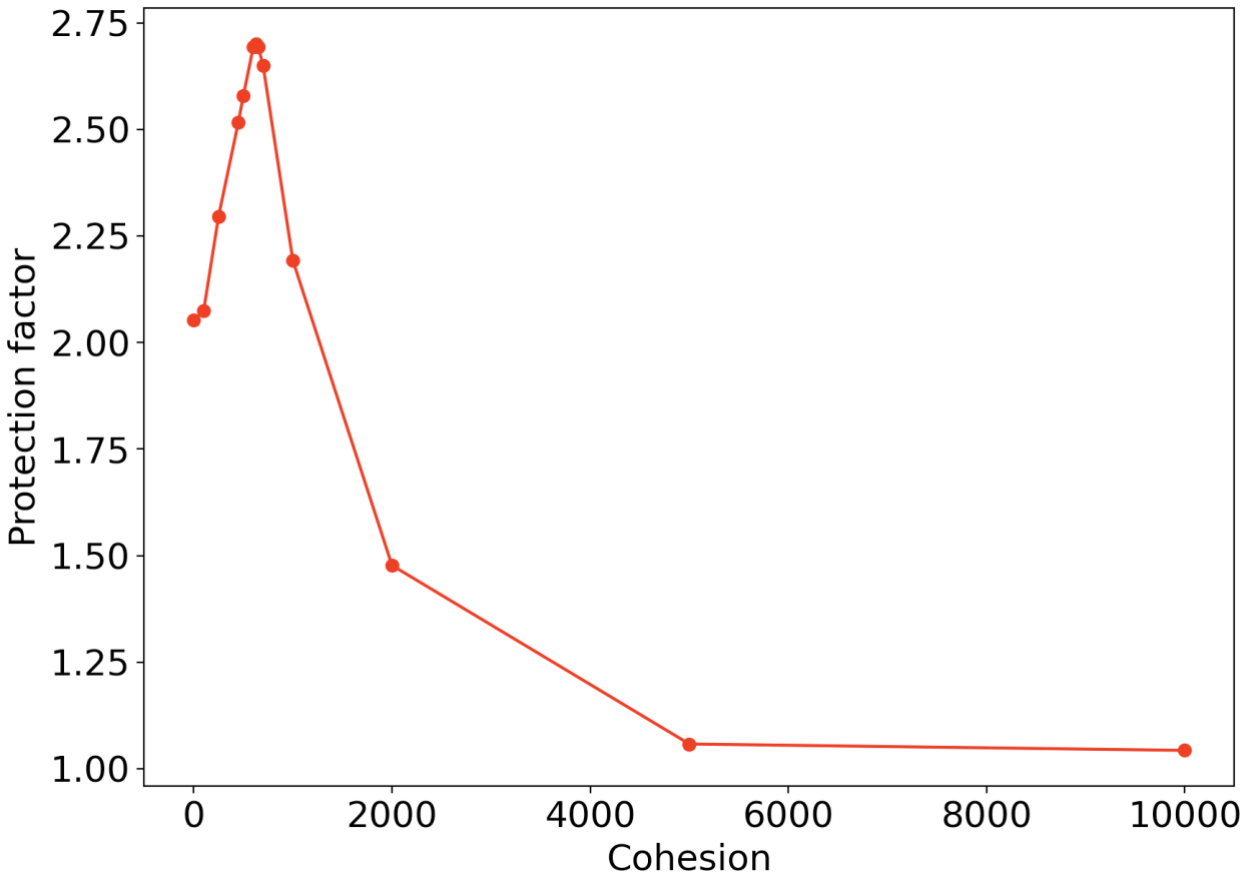

Figure 5. Barrier protection factor as a function of cohesion value. Cohesion is measured in *KPa*. Friction angle φ =1 deg.

3. Conclusions

The presented review of the most frequently used mechanical models for metamaterials in seismic protective barriers and pads, reveals several principally different approaches based on (a) hyperelastic potentials allowing modelling the experimentally observed bi-modularity of granular metamaterials at compression and decompression phases, but incapable of modelling hysteretic behaviour; (b) hypoelastic models, that are even more general then hyperelastic ones, but exhibiting the same shortcoming related to the principle incapability of modelling the hysteretic behaviour; (c) models based on hydrodynamic equations along with discrete element methods (DEM) and smoothed particle hydrodynamic (SPH) methods, as the performed review shows, these methods are potentially applicable for modelling hysteretic behaviour by considering either intrinsic viscosity (hydrodynamic models and SPH) or dry friction between particles (DEM), however, currently they are incapable of accounting different elastic moduli at compression and decompression phases; (d) elastic-plastic models are apparently the best suited to encounter both bi-modularity, if the elastic state is modeled by the hyperelastic potentials, and the persistent material yield, observed at the stress level exceeding the internal cohesion.

Considering one of the most frequently used elastic-plastic models, the Mohr – Coulomb plasticity, it should be noted that the performed numerical analysis reveals momentous potential of granular metamaterials as a filling for seismic barriers. It is demonstrated that the material following the Mohr – Coulomb model can significantly outperform any linear elastic material in terms of reduction of vibrations induced by a seismic source or remote dynamic loading. The analyzed effect of cohesion and friction angles reveals a possibility for prediction of optimal granular metamaterial properties, ensuring maximum possible protection, based on the expected pattern of a seismic or a vibration load.

Acknowledgements

The research is funded by the Ministry of Science and Higher Education of the Russian Federation as part of World-class Research Center program: Advanced Digital Technologies (contract No. 075-15-2020-934 dated 17.11.2020)

References

1. Earle, S. *Physical Geology*, Victoria: B.C., 2015, p.716
2. Krödel S, Thomé N and Daraio C. Wide band-gap seismic metastructures, *Extreme Mech Lett* 2015; 4:111–117.
3. Yousef B and Bertero VV. *Earthquake Engineering: From Engineering Seismology to Performance-Based Engineering*. CRC Press: N.Y., 2004, p.976
4. Woods RD. Screening of surface waves in soils. *J Soil Mech Found Div Proc ASCE* 1968; 94(4): 951–979.
5. Ugalde D, Almazán JL, Santa María H. et al. Seismic protection technologies for timber structures: a review. *Eur J Wood Prod* 2019; 77:173–194.
6. Park D, Jeon B and Deon S. A numerical study on the screening of blast-induced waves for reducing ground vibration. *Rock Mech Rock Eng 2009;* 42: 449–473.
7. Adam M and Estorff O. Reduction of train-induced building vibrations by using open and filled trenches. *Comp Struct* 2005; 83(1):11–24.
8. Brammer AJ. Human response to vibration and mechanical shock. *Canadian Acoustics* 2002; 30(3):112–113.
9. Hunt HEM. *Measurement and Modeling of Traffic-induced Ground Vibration*, PhD thesis, University of Cambridge, UK, 1998.
10. Watts GR.The generation and propagation of vibration in various soils produced by the dynamic loading of load pavements. *J Sound Vibr* 1992; 156(2):191–206.
11. Djeran-Maigre I et al. Solitary SH waves in two-layered traction-free plates. *Comptes Rendus Mécanique* 2008; 336: 102–107.
12. Ilyashenko A et al. SH waves in anisotropic (monoclinic) media. *Z. Angew Math Phys* 2018; 69: 17.
13. Kuznetsov SV. Love waves in layered anisotropic media. *J Appl Math Mech* 2006; 70(1): 116–127.
14. Kuznetsov SV. Fundamental and singular solutions of Lamé equations for media with arbitrary elastic anisotropy. *Quart Appl Math* 2005; 63(3): 455–467.
15. Bratov VA et al. Homogeneous horizontal and vertical seismic barriers: mathematical foundations and dimensional analysis. *Mater Phys Mech* 2020; 44(1): 61–65.
16. Dudchenko AV et al. Vertical wave barriers for vibration reduction, *Arch Appl Mech* 2021; 91: 257–276.

17. Jesmani M, Fallahil MA and Kashani HF. Effects of geometrical properties of rectangular trenches intended for passive isolation in sandy soils. *Earth Sci Res* 2012; 1(2): 137–151.
18. Li S et al. Benchmark for three-dimensional explicit asynchronous absorbing layers for ground wave propagation and wave barriers. *Comp Geotech* 2021; 131: 103808.
19. Li S et al. Explicit/implicit multi-time step co-simulation in unbounded medium with Rayleigh damping and application for wave barrier, *Europ J Env Civil Eng* 2020; 24: 2400–2421.
20. Kuznetsov SV. Seismic waves and seismic barriers, *Acoust Phys* 2011; 57(3): 420–426.
21. Muhammad, Lim CW and Reddy JN. Built-up structural steel sections as seismic metamaterials for surface wave attenuation with low frequency wide bandgap in layered soil medium. *Eng Struct* 2019; 188: 440–451.
22. Pu X and Shi Z. Surface-wave attenuation by periodic pile barriers in layered soils, *Construct Build Mater* 2018; 180: 177–187.
23. Cheng ZB and Shi ZF. Composite periodic foundation and its application for seismic isolation. *Earthquake Eng Struct Dynam* 2017; 47(4): 925–944.
24. Kravtsov AV et al. Finite element models in Lamb's problem. *Mech Solids* 2011; 46: 952–959.
25. Kim SH and Das MP Artificial seismic shadow zone by acoustic metamaterials. *Modern Phys Lett B* 2013; 27(20):1350140.
26. Tsang HH. Seismic isolation by rubber–soil mixtures for developing countries. *Earthquake Eng Struct Dynam* 2007; 37(2): 283–303.
27. Mandal P and Somala SN Periodic pile-soil system as a barrier for seismic surface waves. *SN Appl Sci* 2020; 2: Paper 1184.
28. Pu X and Shi Z Surface-wave attenuation by periodic pile barriers in layered soils. *Construct Build Mater* 2018; 180: 177–187.
29. Guin J and Banerjee PK Coupled soil–pile–structure interaction analysis under seismic excitation. *J Struct Engng, ASCE,* 1998; 124(4): 434–444.
30. Bratov V et al. Seismic barriers: theory and numerical simulations. E3S Web Conf, 2019; 97: Paper 03005.
31. Dudchenko AV et al. Pile rows for protection from surface waves. In: Akimov P., Vatin N. (eds) Proceedings of FORM 2021. *Lecture Notes in Civil Engineering*, 2022; 170: 1-11.
32. Aki K and Richards PG. *Quantitative Seismology*, 2nd ed. University Science Books: Sausalito, California. 2002, p. 685.
33. Nedderman RM. *Statics and Kinematics of Granular Materials*, Cambridge Univ. Press: Cambridge. 2005, p.352.
34. Ericksen JL. *Tensor Fields*. In: Handbuch der Physik, vol. III/1, ed. by S. Flügge, Springer: Berlin. 1960, pp. 794-858.
35. Jackson R. Some mathematical and physical aspects of continuum models for the motion of granular materials, In: R.E. Meyer (Ed.), *Theory of Dispersed Multiphase Flow*, Academic Press: San Diego, 1983, pp. 291–337.
36. Niemunis A and Cudny M. On hyperelasticity for clays. *Comput Geotech* 1998; 23(4): 221-236.
37. Truesdell C. Remarks on hypo-elasticity, *J Res Nat Bur Stand* 1963; B67: 141–143.
38. Gurtin ME. On the hypoelastic formulation of plasticity using the past maximum of stress. *ASME J Appl Mech* 1983; 50: 894–896.
39. Boisse P et al. Hypoelastic, hyperelastic, discrete and semi-discrete approaches for textile composite reinforcement forming, *Int J Mater Forming* 2009; 3(S2): 1229–1240.
40. Hashiguchi K. Hypo-elastic and hyper-elastic equations of soils, *Int J Num Anal Meth Geomech* 2018; 42(13): 1554–1564.

41. Brey JJ et al. Hydrodynamics of an open vibrated granular system, *Phys Rev Ser E* 2001; 63: 061305.
42. Dahl SR et al. Kinetic temperatures for a granular mixture, *Phys Rev Ser E* 2002; 66: 041301.
43. Huang K et al. Dynamic behaviors of supersonic granular media under vertical vibration, *Ultrasonics* 2006; 44: E1487.
44. Goldstein A and Shapiro M. Mechanics of collisional motion of granular materials. I. General hydrodynamic equations, *J Fluid Mech* 1995; 282: 75–114.
45. Torres LA. *Hydrodynamic Modeling of Granular Materials*, PhD thesis. Friedrich-Alexander-Universitat: Erlangen-Nurnberg. 2017.
46. Xiong H et al. A novel multi-scale large deformation approach for modelling of granular collapse. *Acta Geotech* 2021; 16: 2371–2388.
47. Chapman S and Cowling TG. The Mathematical Theory of Nonuniform Gases, Cambridge University Press: London. 1970, p. 447.
48. Bougie J, Moon SJ, Swift JB and Swinney H. Shocks in vertically oscillated granular layers, *Phys Rev Ser E* 2002; 66: 051301.
49. Rericha EC, Bizon C, Shattuck MD and Swinney HL. Shocks in supersonic sand, *Phys Rev Lett* 2001; 88: 014302.
50. Jop P. Rheological properties of dense granular flows, *Comptes Rendus Phys* 2015; 16: 62–72.
51. Kermani E and Qiu T. Simulation of quasi-static axisymmetric collapse of granular columns using smoothed particle hydrodynamics and discrete element methods, *Acta Geotech* 2020; 15(2): 423–437.
52. Otsubo M, O'Sullivan C. and Shire T. Empirical assessment of the critical time increment in explicit particulate discrete element method simulations, *Comput Geotech* 2017; 86: 67–79.
53. Rojek J. Contact modeling in the discrete element method. In: A. Popp, P. Wriggers (Eds.), *Contact Model. Solids Part*, vol. 585, Springer: Berlin, 2018, pp. 177–228.
54. Nguyen CT et al. A new SPH-based approach to simulation of granular flows using viscous damping and stress regularization. *Landslides* 2017; 14(1): 69–81.
55. Peng C et al. Loquat: an open-source GPU-accelerated SPH solver for geotechnical modelling. *Acta Geotech* 2019; 14(5): 1269–1287.
56. Wang G, Riaz A and Balachandran B. Smooth particle hydrodynamics studies of wet granular column collapses. *Acta Geotech* 2019; 15: 1–13.
57. Deng N et al. On the attraction power of critical state in granular materials. *J Mech Phys Solids* 2021; 149: 104300.
58. Liu J et al. Macroscopic softening in granular materials from a mesoscale perspective. *Int J Solids Struct* 2020; 193–194: 222–238.
59. Sawicki A, Sławińska J and Mierczyński J. Structure and calibration of constitutive equations for granular soils. *Studia Geotech Mech* 2015; 36(4): 35–46.
60. Wautier A et al. Multiscale modelling of granular materials in boundary value problems accounting for mesoscale mechanisms. *Comp Geotech* 2021; 134: 104143.
61. Anastasopoulos I, Gazetas G, Loli M et al. Soil failure can be used for seismic protection of structures. *Bull Earthquake Eng* 2010; 8: 309–326.
62. Andrianopoulos KI, Agapoulaki GI and Papadimitriou AG Simulation of seismic response of passively stabilised sand. *Geotech Res* 2016; 3(2): 40–53.
63. Coop MR. The mechanics of uncemented carbonate sands. *Géotechnique* 1990; 40(4): 607–626.
64. Fu P and Dafalias YF. Fabric evolution within shear bands of granular materials and its relation to critical state theory. *Int J Numer Analyt Methods Geomech* 2011; 35(18): 1918–1948.

65. Goldstein RV et al. The modified Cam-Clay (MCC) model: cyclic kinematic deviatoric loading. *Arch Appl Mech* 2016; 86: 2021–2031.
66. Goodman MA and Cowin SC. A continuum theory for granular materials. *Arch Rational Mech Anal* 1977; 44: 250–267.
67. Massoudi M and Mehrabadi MM. A continuum model for granular materials: Considering dilatancy and the Mohr – Coulomb criterion. *Acta Mech* 2001; 152: 121–138.
68. Rajchenbach J. Flow in powders: From discrete avalanches to continuum regime. *Phys Rev Lett* 1990; 65: 2221–2224.
69. LS-DYNA. LS-DYNA Manual R12.0, Livermore Software Technology (LST), An Ansys Company. 2020.